AIMS Materials Science, 11(2): 200–215.
DOI: 10.3934/matersci.2024011
Received: 08 December 2023
Revised: 19 January 2024
Accepted: 02 February 2024
Published: 18 February 2024

http://www.aimspress.com/journal/Materials

Research article

Study of protective hard coatings of SiO_2-TiO_2 on aluminum substrates

Johana Gamez[1], Luis Reyes-Osorio[1,*], Oscar Zapata[1], Roberto Cabriales[1], Luis Lopez[1] and Miguel Delgado-Pamanes[2]

[1] Universidad Autónoma de Nuevo León, Facultad de Ingeniería Mecánica y Eléctrica, San Nicolás de los Garza, México
[2] Instituto Politécnico Nacional, UPIIZ, Profesional Genérica Ingeniería Mecatrónica, Zacatecas, México

* **Correspondence:** Email: luis.reyessr@uanl.edu.mx; Tel: +52-811-016-5901.

Abstract: Aluminum alloys are frequently employed in the aeronautics industry due to the remarkable mechanical properties and lightweight nature of these materials. Moreover, thin film coatings are commonly applied in order to improve the corrosion resistance under harsh environments. In this work, Al 7075-T6 substrates were coated with nanostructured SiO_2-TiO_2 films using a sol-gel method. The experimental approach initially consisted in the preparation of a precursor agent using tetraethyl orthosilicate (TEOS) and triethoxy(octyl)silane (ETOS). Subsequently, nanoparticles of SiO_2-TiO_2 were mixed in order to develop thin films using a one-step dip coating method. The roughness, nanoindentation and corrosion properties were evaluated for the coated substrates. A finite element model was created for the nanoindentation test, which determined the mechanical response between the film-contact interface during loading conditions. The average hardness, elastic modulus and critical loads leading to fracture were verified. The nanoindentation test presented a significant increase in hardness for the coated Al 7075-T6 alloy, reaching a value of 4.6 GPa. The SiO_2-TiO_2 thin films presented uniform and compact surface coatings with high mechanical properties. Furthermore, the performed corrosion tests indicated moderate protection by the SiO_2-TiO_2 thin films. The SiO_2-TiO_2 thin films displayed a generalized corrosion throughout the surface, presenting oxides and fractured crystals in localized regions.

Keywords: nanoindentation; finite element method; Al 7075-T6 alloy; sol-gel; SiO_2-TiO_2

1. Introduction

Aluminum alloys, such as Al 7075-T6, have been frequently applied in the fuselage and panel frames of aircraft due to a combination of high mechanical strength, moderate tenacity and good corrosion resistance [1]. High strength Al alloys present outstanding properties as structural components, but surface treatments must be applied in order to improve the corrosion resistance properties [2]. The use of protective coating must be based on the heat treatment conditions. For instance, the Al 7075-T6 is an age hardened alloy, thus, a high temperature treatment of the coating could decrease its mechanical properties. The development of TiO_2 coatings has been recently studied, which present chemical stability as well as good wear and heat resistance [3]. Soklic et al. [4] used TiO_2 coatings for environmental applications, resulting in coatings with good antifogging, self-cleaning, and antimicrobial surface due to the photocatalytic properties and photo-induced superhyprophilicity of the material.

The effect of aging time on the structural and chemical properties of SiO_2-TiO_2 composite was investigated by Comakli et al. [5]; the SiO_2-TiO_2 films were developed using the sol-gel technique. A better corrosion resistance for the SiO_2-TiO_2 films was determined and the aging time was found to considerably affect the corrosion properties of the composite coatings. Gobara [6] used SiO_2-TiO_2 nanoparticles to develop coatings with enhanced mechanical properties. The sol-gel technique was applied to generate the SiO_2-TiO_2 thin films on Al 3003 substrates and the influence of nanoparticles on adhesive strength was investigated. The addition of TiO_2 allowed to increase the adhesion performance and moreover, the hydrophobic characteristics were improved by the addition of SiO_2 nanoparticles. Krishna et al. [7] developed a single and multilayer SiO_2-TiO_2 film applied in mild steel by a sol gel technique and observed a reduction of oxidation for the multilayer film due to the effective coverage between coatings. In this study, we reported that the addition of SiO_2 to TiO_2 minimized the coating defects. Khosravi et al. [8] developed a multilayer SiO_2-TiO_2 coating on a low-cost commercial steel, in which the effect of number of layers, annealing temperature, and atmosphere were evaluated. The results indicated that increasing the annealing temperature reduced surface fracture. Jacobs et al. [9] generated SiO_2/TiO_2 thin films by spray coating and reported good adhesion when SiO_2 was added to the TiO_2 coating. Widati et al. [10] dip-coated glass substrates with SiO_2/TiO_2 films. It was observed that SiO_2 and TiO_2 composites increase the surface roughness of the coating, but there is a decrease of transparency of the substrate. Recently, hybrid coatings on carbonyl iron particles have been developed by sol-gel method to promote better magnetic and thermal stability. The hybrid layer improves the corrosion resistance inhibiting the diffusion of corrosive medium [11–13].

On the other hand, mechanical testing using nanoindentation equipment allows us to evaluate mechanical parameters of bulk and films at submicron size [14,15]. Alaboodi and Hussain [16] described a detailed review of nanoindentation experiments and a finite element procedure to evaluate thin films. Commonly, nanoindentation measurements are developed using Berkovich indenters by the Oliver and Pharr methodology. This method considers the material as homogeneous, continuous and isotropic [17]. The finite element method (FEM) has been used to determine the mechanical response of thin film coatings by simulating the process of nanoindentation [18,19]. Through FEM, the induced deformation and stress distribution can be determined in a direct manner [20,21]. For example, Chen et al. [22] studied the mechanical response of thin film coatings by finite element method. The induced stress distribution of thin films was recorded using different indenters, such as Berkovich, spherical and flat indenters. Lichinchi et al. [23] developed thin films of TiN on steel substrates. A finite element procedure was performed using a Berkovich indenter. It was observed that no apparent differences

exist between the experimental load-displacement curves and those obtained from a 2D axisymmetric numerical model. Wang et al. [24] conducted nanoindentation experiments to evaluate the impact of residual stress on laminar plasma quenched materials.

Different approaches have been suggested to evaluate elastic properties from indentation load-displacement data. For example, Kang et al. [25,26] developed a linear optimization approach to improve the accuracy of mechanical properties. A good agreement was observed for the elastic properties of a single loading-unloading curve. In addition, Noii and Aghayan [27] determined the elastic-plastic material properties of hydroxyapatite coatings on different substrates. A global optimization approach was performed using the load-displacement data. In this work, an experimental and numerical study was developed to determine the mechanical and corrosion properties of sol-gel nanostructured SiO_2-TiO_2 thin films. The performed corrosion tests in the coated Al 7075-T6 substrates indicate moderate protection by the SiO_2-TiO_2 thin films. A finite element model was proposed to determine the average hardness, elastic modulus and critical loads that lead to fracture. The 2D axisymmetric model corroborates the experimental nanomechanical properties of SiO_2-TiO_2 thin film coatings.

2. Materials and methods

2.1. Experimentation

The Al 7075-T6 alloy part was sectioned and polished to obtain square plates of 25 mm of length with a thickness of 7 mm. A superficial analysis by EDX was performed to obtain the main alloying elements of Al 7075-T6 alloy (Al 85.45%, Mg 3.1%, Zn 6.15%, and Cu 5.25%). The Al substrate was characterized by optical microscopy through a ZEISS observer Z1 light microscope and an electron microscopy scanner JEOL JSM-6510LV for the morphological characterization of the coatings.

A sol-gel procedure was used for the preparation of the coatings. One of the fundamental parts of this process is the solution in which the specimens were immersed. This mixture was made into two phases: the first phase consists of preparing the precursor agent, which agent combines tetraethyl orthosilicate (TEOS) and triethoxy(octyl)silane (ETOS), in quantities of 22 and 25 mL, respectively. The mixture was agitated in an ultrasonic bath after a lapse of 20 min. For the second phase, a mixture was generated with the following reactive elements: nanoparticles of titanium dioxide and silicon dioxide (SiO_2-TiO_2), deionized water and nitric acid (HNO_3), in quantities of 0.048 g, 5 mL, and 0.3 mL, respectively; 3 wt.% of SiO_2 nanoparticles. The precursor was dissolved into a mixture of SiO_2-TiO_2, H_2O and HNO_3 and was agitated in an ultrasonic bath for a lapse of 30 min. At the end of the process a homogeneous mixture was obtained and placed inside a dip-coating equipment, which was programmed with the necessary length for the Al samples to be totally coated by the immersion process. The speed at which the samples were introduced into the mixture was 10 mm/s and the withdraw velocity was 1 mm/s, as shown in Figure 1.

Figure 1. Coated samples by the immersion-removal process at inlet velocity of 10 mm/s.

After dip-coating, a heat treatment was carried out on the samples consisting in two stages. The first stage was a pre-heating, in which the samples were placed inside a Felisa oven at a temperature of 180 °C for 10 min. Subsequently, the second stage consisted in placing the samples in a Thermo Scientific oven for 2 h under a temperature at 300 °C. Samples were analyzed by a scanning electronic microscope to observe the homogeneity of the coating. Keller reagent was used to reveal the microstructure of the substrates. The samples were prepared using 95 mL of distilled water, 1 mL of hydrofluoric acid (HF), 1.5 mL of hydrochloric acid (HCl), and 2.5 mL of nitric acid (HNO_3).

Surface roughness measurements were performed using a CounturGT Bruker profilometer in order to evaluate the morphology and homogeneity of the coating within substrate in different sections. The surface profiling with white light interferometry provides highly accurate topographic information about the surface of a sample. Multiple interference patterns are generated reconstructing a detailed 3D map of the height variations, surface roughness and shape details. A step from an uncoated to a coated area is considered in order to determine the step height and therewith the coating thickness.

On the other hand, to analyze the mechanical behavior of the nanostructured coating, nanoindentation tests were performed using CSM Instruments Nanoindentator with a Berkovich indenter. The operational parameters are shown in Table 1. Twenty indentations were performed with a partition of 20 μm.

Table 1. Operational parameters of the nanoindentation test.

Parameters	Coated substrate	Uncoated substrate
Load (mN)	40	50
Velocity (mN/min)	80	100
Deposition time (s)	2	2

The nanoindentation parameters for the coating samples were modified due to the mechanical and chemical properties of the ceramic films. It was observed that loads higher than 50 mN presented

damage and fractures in the coating. The selected parameters were defined based on a series of tests along the surface.

Two corrosion tests were performed in the thin coatings: polarization resistance (RP) and electrochemical impedance spectroscopy (EIS). In order to carry out the RP and EIS tests, a frequency range of 0.01 Hz to 50 kHz with a sweep speed of 0.1 mV/s was defined. A measuring range of 10 decades was considered in the study. The procedure was developed using a Solartron SI 1287 electrochemical interface and a Solartron SI 1260 impedance gain-phase analyzer. An electrochemical cell was used to evaluate the interaction between the Al samples and the corrosive agent, considering a solution of 3.5% NaCl by weight percent. The tests were performed under a three-electrode system; the working electrode (Al 7075-T6), the reference electrode (Calomel) and the counter electrode (platinum). The contact area was 1 cm^2 and five replications were performed on each sample to ensure reproducibility. It should be noted that the coated samples were previously immersed for a period of 20 h within the solution of 3.5% NaCl in order to obtain consistent results of the interaction with the SiO_2-TiO_2 coating. Measurements of the samples without coating were performed after 5 min, once it has been mounted in the electrolytic cell in order to have a brief period of stabilization between the corrosive agent and the sample.

2.2. Finite element method

A finite element method was performed to evaluate the mechanical response of SiO_2-TiO_2 layers placed in Al 7075-T6 substrate. The simulations were run in Simufact Forming finite element platform, considering a thickness of 1.12 μm for the SiO_2-TiO_2 thin films. For the indentation process, a Berkovich indenter was selected with an equivalent conical point of 70.3°. Figure 2 shows the discretization characteristics and used geometries to simulate nanoindentation test. In Figure 2a the indenter, Al 7075-T6 substrate and a SiO_2-TiO_2 thin film are observed. In Figure 2b the mesh convergence study is illustrated; the number of elements in the model reach a convergent state after a strain of 1.01. A minimum element size of 0.02 nm was generated to have a sufficiently fine mesh in the contact zone.

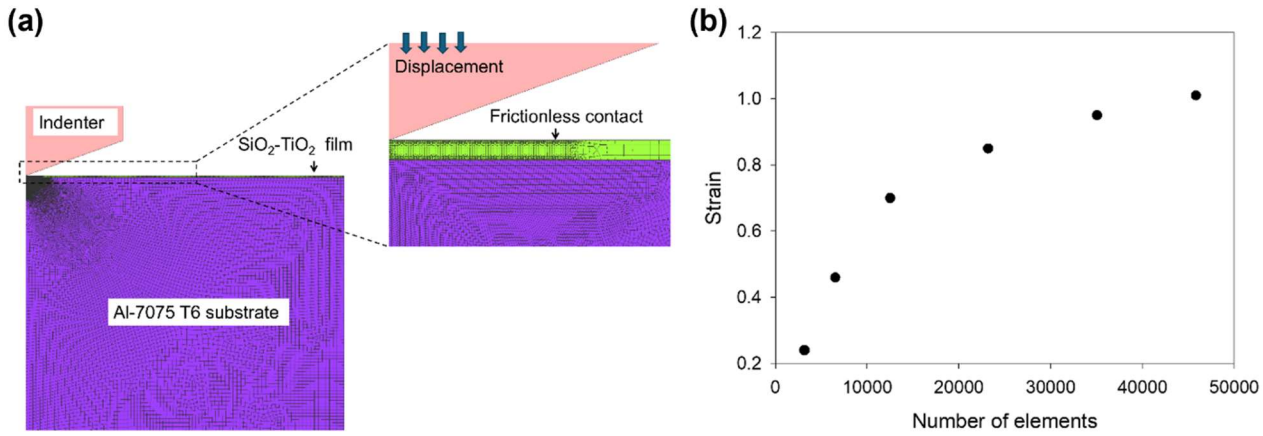

Figure 2. Discretization of numerical model, (a) nanoindentation test, and (b) convergence study.

The numerical model consists of a very refined mesh near the indenter tip due to the large displacement contact associated with nanoindentation procedure. The SiO_2-TiO_2 film consists of 48000 elements, while the substrate includes 15040 elements. The indenter was considered as a rigid body and it is forced into the Al 7075-T6 substrate. Node-to-segment contact was applied for the interaction between indenter and coating. The contact between bodies is perfectly bonded and the friction is considered negligible. A remeshing criteria was activated due to the large deformation condition; this option helps to avoid excessive element distortion. Two steps were created in the numerical model: initially, the indenter has a displacement boundary condition assigned downwards, while in the second step, the indenter is moved upwards and elastic recovery is allowed. At the end of the process, a load-displacement curve is obtained. Table 2 shows the applied material properties in nanoindentation simulation of Al 7075-T6 alloy with SiO_2-TiO_2 thin films.

Table 2. Material properties for nanoindentation test of thin films on Al 7075-T6 substrate [22].

Material	Elastic modulus (GPa)	Poisson ratio
Substrate (Al 7075-T6 alloy)	71.7	0.33
SiO_2-TiO_2 coating	330 [This work]	0.35
Diamond indenter	1141	0.07

The elastic-perfect plastic behavior of SiO_2-TiO_2 coating is included using a bilinear isotropic hardening rule with a tangent modulus of zero. The substrate is considered as an elastic-plastic material in the numerical model [28]. The penetration of the indenter was based on the susceptibility of fracture of the film coating.

3. Results and discussion

The as-received microstructure of the Al 7075-T6 alloy substrate is observed in Figure 3. In Figure 3a it is observed an elongated recrystallized microstructure with second phases (dark points), which influences the mechanical properties of Al 7075-T6 alloy. The T6 heat treatment condition exhibits very fine precipitates within the grains and coarse precipitates closely spaced along grain boundaries [28]. The microstructure observed in Figure 3b is composed mainly of a mixture of Guinier-Preston zones, areas associated with aging hardening phenomenon, and transition precipitates η ($MgZn_2$) according to reported literature [29,30].

Figure 4 presents the EDX spectra of coated and uncoated Al 7075-T6 samples under corrosion conditions. It is observed that the presence of chlorine peak generates due to a corrosive medium.

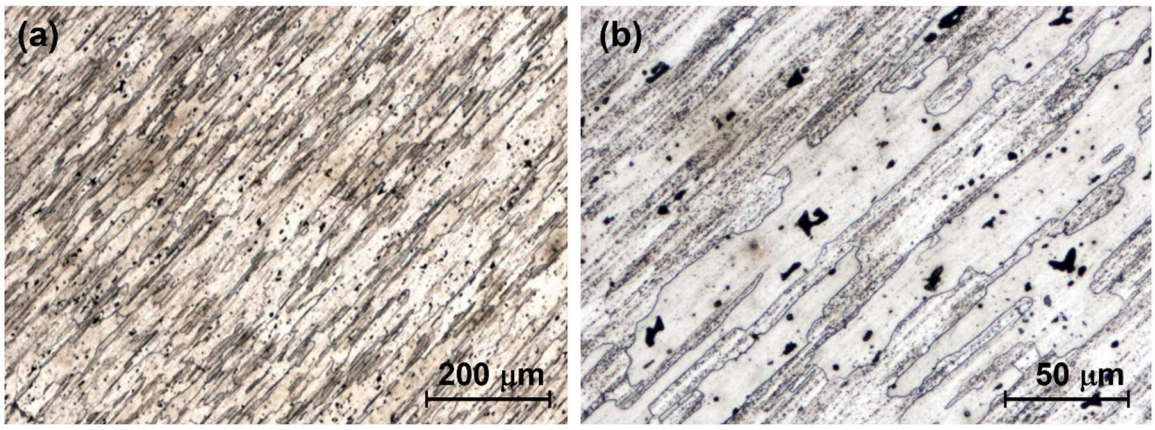

Figure 3. Al 7075-T6 substrate chemically attacked by Keller's reagent, (a) 5× and (b) 20× magnification.

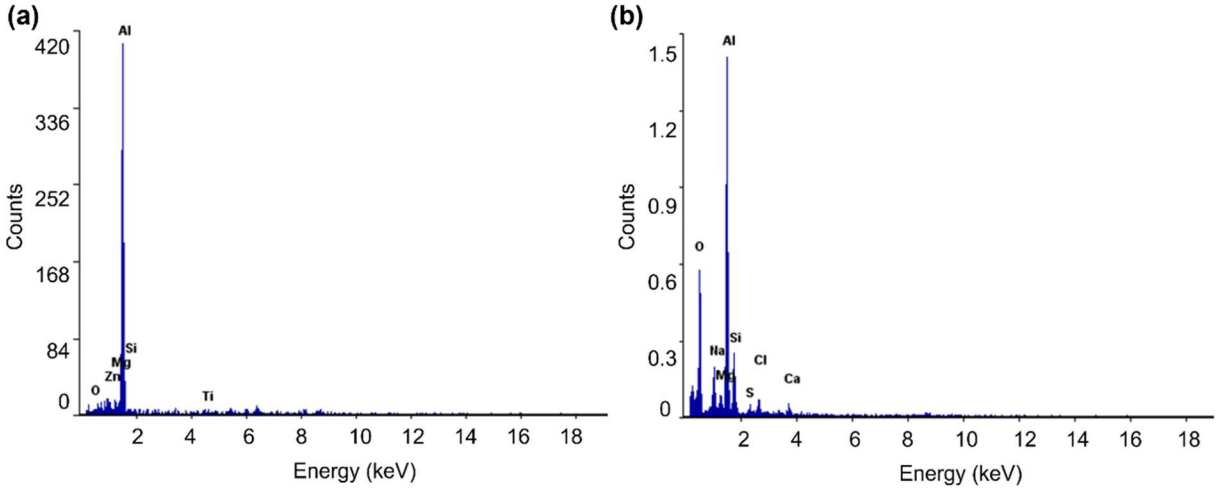

Figure 4. EDX spectrum of samples under corrosion. (a) Samples of bare Al 7075-T6 alloy, and (b) samples coated with SiO_2-TiO_2 thin film.

The results of surface roughness measurements are based on the roughness value (Ra) between the analyzed positions, see Figure 5. The step technique was selected to evaluate the thickness value within the substrate. The SiO_2-TiO_2 thin film presented an average thickness of 1.12 μm and Ra of 2.35 μm, while uncoated substrates showed a Ra of 5.36 μm.

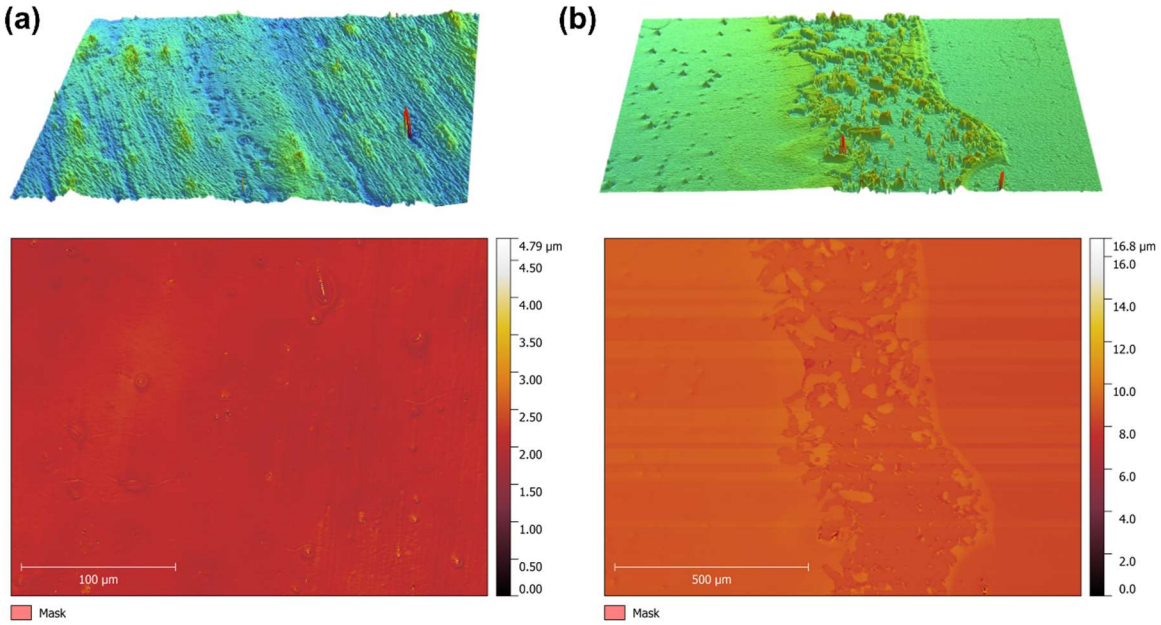

Figure 5. Surface roughness of SiO_2-TiO_2 films on Al 7075-T6 substrates. (a) Average roughness measurements and (b) step used to evaluate the thickness of the substrate.

The determined roughness values agree with previous literature [31]. On the other hand, the mechanical interaction between the SiO_2-TiO_2 film and Al 7075-T6 substrate is determined by nanoindentation testing and the finite element method. Figure 6 shows the experimental and simulated values of the load-displacement curve of coated substrates after 20 indentations. A normal force is applied, and the resultant penetration is recorded based on the initial contact surface. In general, there is a good agreement between experimental and numerical results. However, the indentation curve starts to deviate and becomes lower than experimental curve.

The finite element results reproduce the multiple-step characteristic of the loading section. This behavior is related to elastic–plastic deformation and associated dislocation features. For coated samples, the deviation of the simulated indentation load becomes slightly higher than the experimental value as the indentation depth is beyond 500 nm. This could be associated with regions beneath the indenter which transformed to less deformable structure in the film [22]. In addition, the finite element simulation considers that the mechanical properties of SiO_2-TiO_2 film remain unchanged.

The nanoindentation results showed a significant increase in hardness for the coated Al 7075-T6 alloy, resulting in an average hardness value of 4.6 GPa, which is twice higher than the uncoated samples. Additionally, an increase in the Young's modulus for the coated specimens was determined as well, which indicates that the coating provides better mechanical properties to the substrate. A previous study by Chuang and Luo determined TiO_2 coatings with elastic modulus of 225 GPa for heat treatment conditions at 600 °C [32]. Moreover, Bastakys et al. [33] found that SiO_2-TiO_2 coatings which were deposited by thermal spray presented greater resistance to mechanical wear.

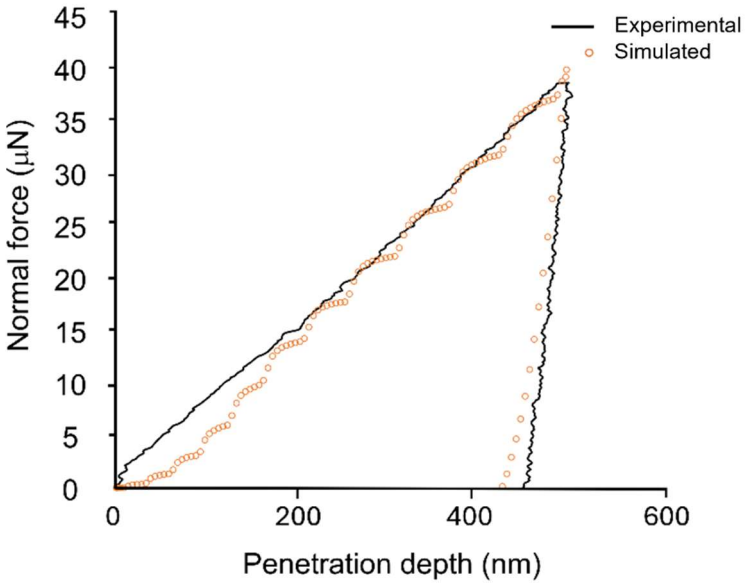

Figure 6. Normal force vs. penetration depth of nanoindentation testing on coated samples.

Figure 7 shows the mechanical behavior of SiO_2-TiO_2 coatings after indentation the test. In Figure 7a, the finite element model shows the stress distribution at the end of the nanoindentation test. The SiO_2-TiO_2 deforms showing a maximum strain of 1.01, see Figure 7b. The maximum value of equivalent stress is 7.4 GPa, which is higher than the experimental results. This can be attributed to the non-linearity of elastic region of the coating near the indenter tip [22]. The stress in thin films occurred during drying and densification process showing increment as heat treatment temperature increases [34]. Figure 7c presents the shear stress distribution of the SiO_2-TiO_2 thin coating with a maximum value of 4.2 GPa. It can be observed that shear stress concentrates near to the contact region between indenter and coating, as well as in the contact region between coating and substrate. Figure 7d presents the principal stress in the axial *Z* direction with a maximum value of 1.3 GPa.

The micrographs of the coated and uncoated Al 7075-T6 substrate under standard and corroded conditions are shown in Figure 8. It is observed that a generalized corrosive attack occurred in both conditions, which is intensified in certain areas due to accumulations of the corrosive agent and some superficial deterioration.

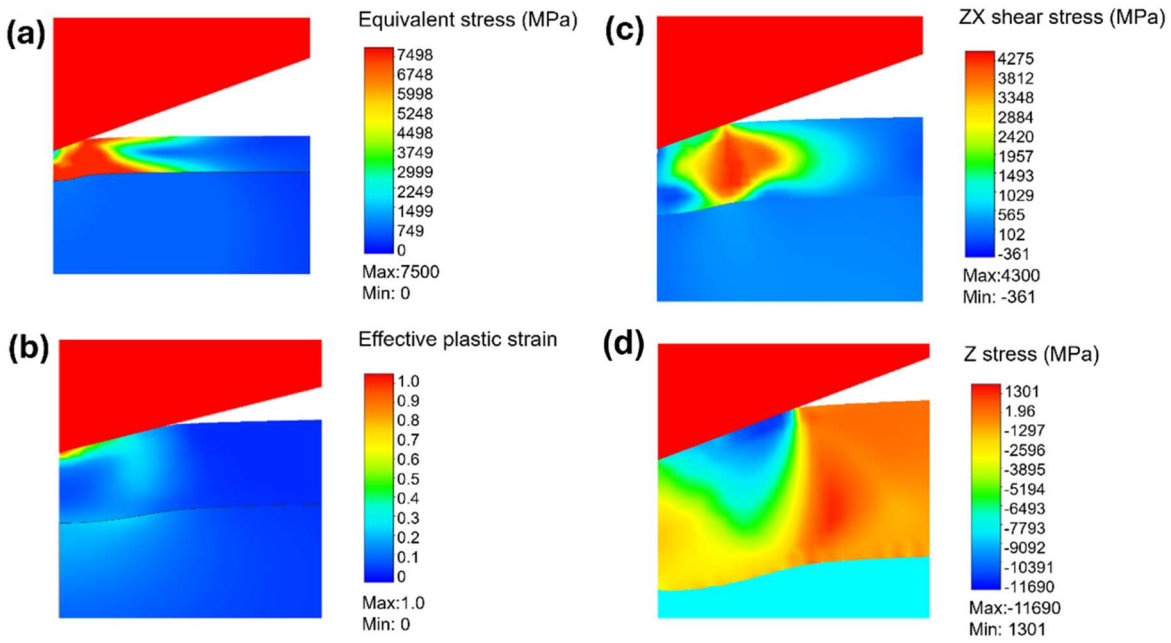

Figure 7. Numerical results of SiO_2-TiO_2 thin films. (a) Equivalent stresses (MPa) at the end of the indentation, (b) equivalent plastic strain after removing the indenter (springback), (c) shear stress distribution (MPa), and (d) principal stress in *Z* direction (MPa).

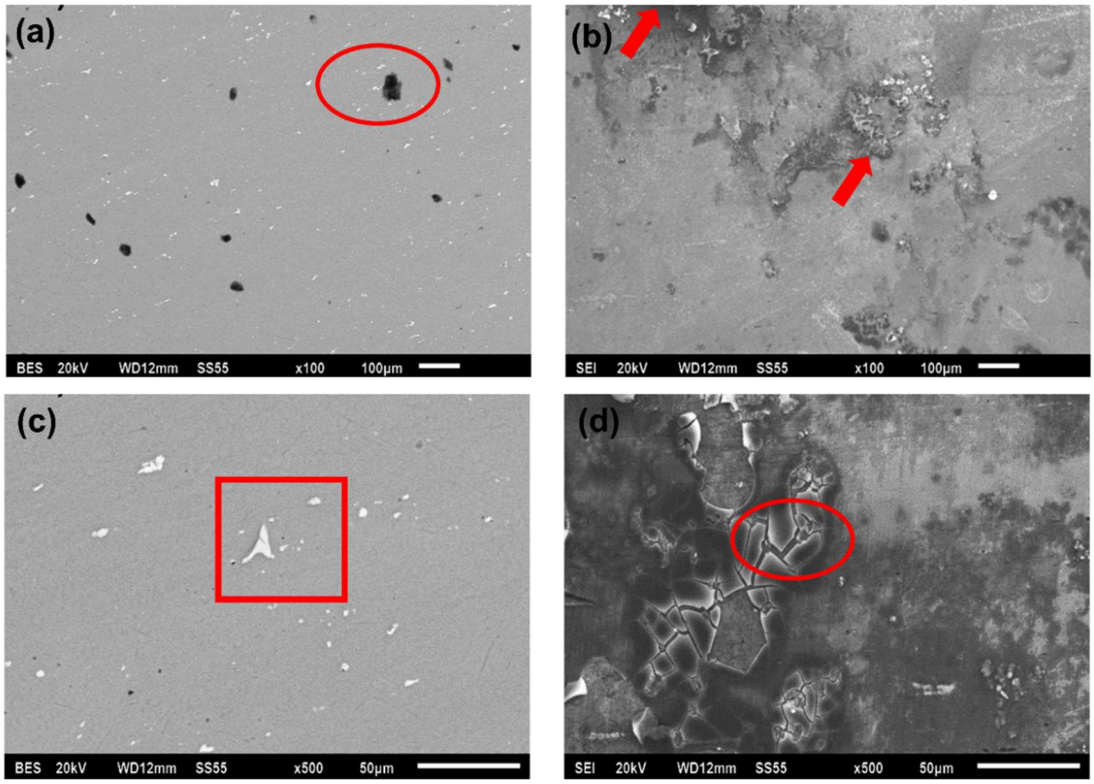

Figure 8. Micrographs of SiO_2-TiO_2 thin films deposited by sol gel method, (a) standard uncoated substrate (100×), (b) corroded uncoated substrate (100×), (c) standard coated Al 7075-T6 substrate, and (d) corroded coated Al 7075-T6 substrate (500×).

Two types of precipitates are observed in Figure 8a; the darker precipitate (oval mark) with Mg and Si inclusions generates the Mg_2Si phase, while the lighter precipitate with Cu and Fe inclusions generates the Al_7Cu_2Fe phase in the substrate under standard conditions. Likewise, Figure 8b shows the substrate under corrosion conditions. A generalized attack throughout the surface is observed, which presents regions of aluminum oxides (square mark) and fractured crystals of the salts only on certain areas. Moreover, Figure 8c,d show the corrosion effects of coated Al 7075-T6 substrates. These conditions presented a generalized corrosion together with certain areas where localized corrosive attack occurred. This effect is reflected in the severe damage to the substrate with the presence of sulfides and chlorides. Table 3 shows the polarization resistance of coated and uncoated Al 7075-T6 alloy. From the PR test, an average corrosion rate of 0.064 mm/year for the coated substrate was determined, while the Al 7075-T6 substrate presented a corrosion rate of 0.0738 mm/year. This is exposed in the average corrosion resistance; in the coated substrate it is 4595.56 $\Omega \cdot cm^2$ while in the Al 7075-T6 substrate it is 3792.46 $\Omega \cdot cm^2$.The coated substrate shows a higher resistance to corrosion compared to the uncoated samples. This effect could be associated with the coating adhesion in the substrate, although the coating was homogeneously distributed throughout the film, a higher concentration in certain areas of the surface was observed. The corrosion mechanism of Al-7075 T6 coated with SiO_2-TiO_2 sol-gel coatings is principally controlled by pores or cracks in the thin films.

Table 3. Polarization resistance of coated and bare Al 7075-T6 substrate.

Parameters	Uncoated substrate	Coated substrate
Corrosion (mm/year)	0.0738	0.064
Polarization resistance ($\Omega \cdot cm^2$)	3792.46	4595.56
Voltage (V)	–0.892	–0.802

It has been observed that the corrosion performance of the SiO_2-TiO_2 coatings can be improved with proper attention on the substrate surface (polishing) before applying the coating. The SiO_2-TiO_2 films obtained in this work were developed in a single layer, which may have intervened in the results of resistance to linear polarization. It has been previously demonstrated that in bilayer systems, the polarization resistance of the coating increases with respect to the uncoated substrate [35]. Rivero et al. [36] demonstrated as well that a thicker coating presents a better corrosion resistance compared with a single dip-coating process. Shadravan et al. [37] observed that a 3-layer coating in Al alloy with 15 wt.% of carbon nanotubes has an outstanding resistance against corrosion in a NaCl (3.5%) solution.

Figure 9 shows the Nyquist plot for coated (point symbol) and uncoated (square symbol) Al 7075-T6 samples. The resistance is determined using the diameter of the semicircles, where a large diameter is associated with a low corrosion growth rate and high corrosion resistance. Additionally, the higher values of Z modulus are presented at lower frequencies, which involves a greater corrosion resistance of the samples.

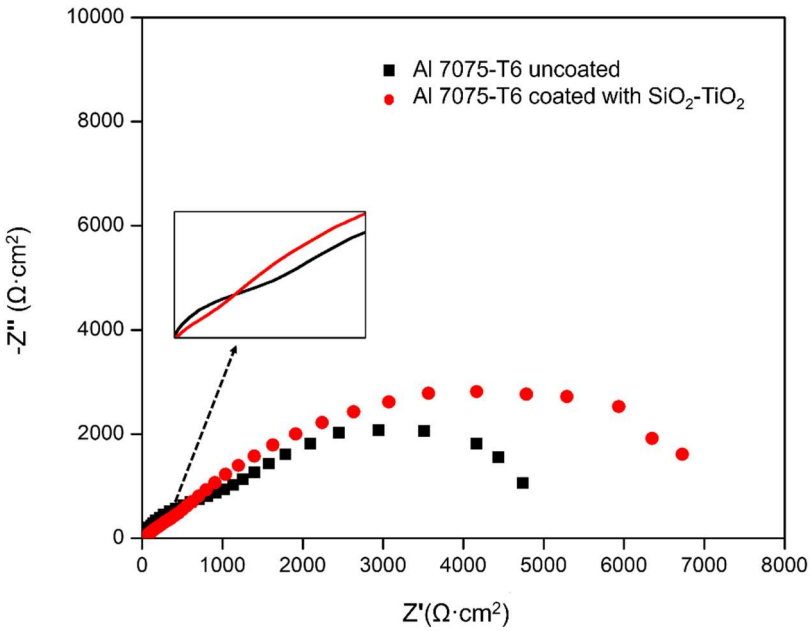

Figure 9. Electrochemical impedance spectroscopy test of coated and uncoated Al 7075-T6 substrates.

Two-time constants are observed for the uncoated sample; the first one refers to the natural passivation layer of the material which presents a diameter of 2100 $\Omega \cdot cm^2$. The second constant refers to the resistance to the charge transfer in the substrate; this is the interaction of the electrolyte with the metal which presents a value of 2950.58 $\Omega \cdot cm^2$. For both coated and uncoated conditions, a capacitive behavior occurs in the high-frequency zone. However, the coated samples maintain the same behavior (capacitive) until closing the semicircle at 7500.79 $\Omega \cdot cm^2$ without showing any semicircle despite of different exposed conditions.

According to the EIS results, there is a moderate effectiveness of the SiO_2-TiO_2 coating applied to the substrate. The generated semicircle in the coated sample has a charge transfer greater than the uncoated substrate (magnitude of the diameter of the semicircles), as well as a capacitive behavior in the areas of high frequency. There is an inductive behavior between 900 and 1000 $\Omega \cdot cm^2$ for the uncoated samples. This results in a second semicircle, mostly pronounced, which may be associated with the interaction of the passivation layer formed by the substrate and the corrosive agent. The impedance results were collected based on a simulation of an equivalent electrical circuit using the Zview software, as shown in Figure 10.

The circuit of Figure 10a presents the results of one-time constant. The equivalent electrical circuit includes a resistor RS that represents the solution resistance, a capacitance C1 and a resistance R1, which are in parallel and reflect the resistance of charge transfer at the metal-electrolyte interface. In Figure 10b a circuit with two-time constants is observed, representing two semicircles formed in the Nyquist diagram. The resistance Rs is connected to a resistance R1 and a capacitance CPE1, where the resistance R1 is the resistance of ionic conduction paths. The second capacitor CPE2 and second resistor R2 represent the charge transfer resistance at the metal-electrolyte interface and the capacitance. Therefore, in order to compare the resistances of coated and uncoated substrates, the value R1 from circuit 1 and R2 from circuit 2 are considered.

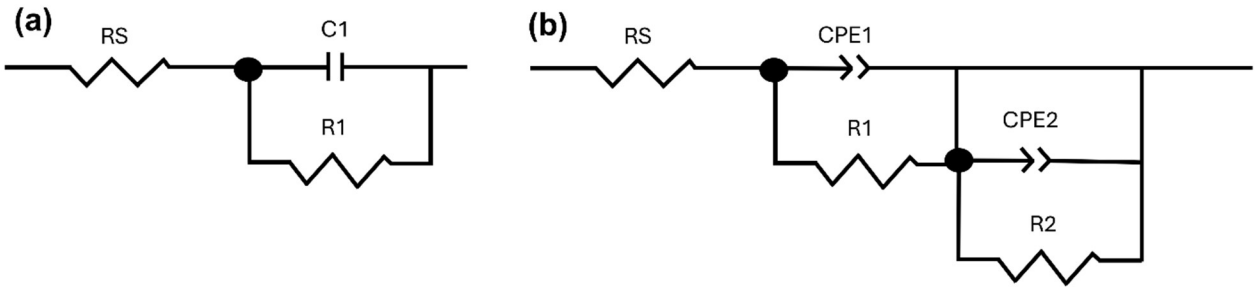

Figure 10. Equivalent electrical circuit, (a) one-time constant, and (b) two-time constants.

The localized corrosion effect is observed in certain areas which presented severe damage under the presence of sulfides and chlorides. It is possible that the heat treatment (300 °C) and the thickness of the coating contributes to the ease of formation of cracks in the coating by which the corrosive agent could be developed with a greater intensity. The results indicate that the oxide layer formed in the alloy has a longer lifetime and is therefore more efficient than one-layer coatings. However, further investigation needs to be developed in this regard. Heat treatment condition could be associated with the development of very fine pores, penetrating the electrolyte and leading to localized corrosion.

4. Conclusions

Thin films of nanostructured SiO_2-TiO_2 were developed by sol gel method on Al 7075-T6 substrates. The sol-gel method presented an easy and cost-effective method for preparation of thin films. A homogenous coating was observed for different samples prepared. SiO_2-TiO_2 coatings were evaluated by nanoindentation showing a hardness value of 4.6 GPa and a Young modulus of 330 GPa. The hardness value is twice higher than in the uncoated samples. The results of the EIS testing show a moderate corrosion effectiveness of the SiO_2-TiO_2 coating applied to the substrate. The generated semicircle in the coated samples has a charge transfer greater than in the uncoated substrate, as well as a capacitive behavior in the areas of high frequency for both conditions, followed by inductive behavior in the vicinity of the real axis. The uncoated samples presented a second semicircle, which may be associated with the interaction of the passivation layer formed by the substrate and the corrosive agent. The finite element method was applied to evaluate the mechanical response of a single layer SiO_2-TiO_2 thin films placed in Al 7075-T6 substrate. The maximum value of equivalent stress by FEM was 7.4 GPa, which can be affected by the non-linearity of elastic region of the coating near the indenter tip. The SiO_2-TiO_2 nanostructured coatings have efficient mechanical and chemical properties, which strengthen the studied Al 7075-T6 substrates.

Use of AI tools declaration

The authors declare that they have not used Artificial Intelligence (AI) tools in the creation of this article.

Acknowledgments

We would like to thank the National Council for Science and Technology of Mexico (CONACyT), Universidad Autónoma de Nuevo León and Instituto Politécnico Nacional.

Conflict of interest

The authors declare no conflicts of interest in this work.

References

1. Liberini M, De Falco G, Scherillo F, et al. (2016) Nano-TiO_2 coatings on aluminum surfaces by aerosol flame synthesis. *Thin Solid Films* 609: 53–61. https://doi.org/10.1016/j.tsf.2016.04.025
2. Immarigeon JP, Holt RT, Koul AK, et al. (1995) Lightweight materials for aircraft applications. *Mater Charact* 35: 41–67. https://doi.org/10.1016/1044-5803(95)00066-6
3. Liu T, Zhang F, Xue C, et al. (2010) Structure stability and corrosion resistance of nano-TiO_2 coatings on aluminum in seawater by a vacuum dip-coating method. *Surf Coat Technol* 205: 2335–2339. https://doi.org/10.1016/j.surfcoat.2010.09.028
4. Soklic A, Tasbihi M, Kete M, et al. (2015) Deposition and possible influence of a self-cleaning thin TiO_2/SiO_2 film on a photovoltaic module efficiency. *Catal Today* 252: 54–60. https://doi.org/10.1016/j.cattod.2014.10.021
5. Çomakli O, Yazici M, Yetim T, et al. (2017) The effects of aging time on the structural and electrochemical properties of composite coatings on CP-Ti substrate. *J Bionic Eng* 14: 532–539. https://doi.org/10.1016/S1672-6529(16)60419-5
6. Gobara M (2015) Effects of TiO_2/SiO_2 reinforced nanoparticles on the mechanical properties of green hybrid coating. *Int Lett Chem Phys Astron* 47: 56–66. https://doi.org/10.56431/p-z14m86
7. Krishna V, Padmapreetha R, Chandrasekhar SB, et al. (2019) Oxidation resistant TiO_2-SiO_2 coatings on mild steel by sol-gel. *Surf Coat Technol* 378: 125041. https://doi.org/10.1016/j.surfcoat.2019.125041
8. Khosravi SH, Veerapandiyan VK, Vallant R, et al. (2020) Effect of processing conditions on the structural properties and corrosion behavior of TiO_2-SiO_2 multilayer coatings derived via the sol-gel method. *Ceram Int* 46: 17741–17751. https://doi.org/10.1016/j.ceramint.2020.04.079
9. Jacobs M, De Vos Y, Middelkoop V (2021) Thickness controlled SiO_2/TiO_2 sol-gel coating by spraying. *Open Ceram* 6: 100121. https://doi.org/10.1016/j.oceram.2021.100121
10. Widati AA, Nuryono N, Kartini I (2019) Water-repellent glass coated with SiO_2-TiO_2-methyltrimethoxysilane through sol-gel coating. *AIMS Mater Sci* 6: 10–24. https://doi.org/10.3934/matersci.2019.1.10
11. Zhang L, Zheng Q, Yin L, et al. (2021) Surface passivation of applying an organic-inorganic hybrid coatings toward significantly chemically stable iron powder. *Colloid Surface A* 610: 125910. https://doi.org/10.1016/j.colsurfa.2020.125910
12. Zhang L, Wan W, Jiang X, et al. (2022) Enhancement of oxidation and corrosion resistance of flaky carbonyl-iron powder via SiO_2/KH560/PDMS coating applied with sol-gel. *Surf Coat Technol* 437: 128346. https://doi.org/10.1016/j.surfcoat.2022.128346

13. Zhang L, Wang B, Jiang X, et al. (2022) Silicone-encapsulated carbonyl iron filler for corrosion-resistant electromagnetic shielding. *Mater Chem Phys* 282: 125918. https://doi.org/10.1016/j.matchemphys.2022.125918
14. Oliver WC, Pharr GM (2004) Measurement of hardness and elastic modulus by instrumented indentation: Advances in understanding and refinements to methodology. *J Mater Res* 19: 3–20. https://doi.org/10.1557/jmr.2004.19.1.3
15. Kalidindi SR, Pathak S (2008) Determination of the effective zero-point and the extraction of spherical nanoindentation stress–strain curves. *Acta Mater* 56: 3523–3532. https://doi.org/10.1016/j.actamat.2008.03.036
16. Alaboodi AS, Hussain Z (2019) Finite element modeling of nano-indentation technique to characterize thin film coatings. *J King Saud Univ Eng Sci* 31: 61–69. https://doi.org/10.1016/j.jksues.2017.02.001
17. Jimenez-Pique E, Gonzalez-Garcia L, Gonzalez-Elipe AR, et al. (2014) Nanoindentation of nanocolumnar TiO_2 thin films with single and stacked zig-zag layers. *Thin Solid Films* 550: 444–449. https://doi.org/10.1016/j.tsf.2013.10.022
18. Bressan JD, Tramontin A, Rosa C (2005) Modeling of nanoindentation of bulk and thin film by finite element method. *Wear* 258: 115–122. https://doi.org/10.1016/j.wear.2004.05.021
19. Zhang W (2017) Mechanical characterization of YBCO thin films using nanoindentation and finite element method. *Int J Mater Res* 108: 732–740. https://doi.org/10.3139/146.111533
20. Mocko W, Szymanska M, Smietana M, et al. (2014) Simulation of nanoindentation experiments of single-layer and double-layer thin films using finite element method. *Surf Interface Anal* 46: 1071–1076. https://doi.org/10.1002/sia.5473
21. Gupta AK, Porwal D, Dey A, et al. (2016) Evaluation of critical depth ratio for soft V_2O_5 film on hard Si substrate by finite element modeling of experimentally measured nanoindentation response. *J Phys D Appl Phys* 49: 155302. DOI 10.1088/0022-3727/49/15/155302
22. Cheng SW, Chen BS, Jian SR, et al. (2022) Finite element analysis of nanoindentation responses in Bi_2Se_3. *Coatings* 12: 1554. https://doi.org/10.3390/coatings12101554
23. Lichinchi M, Lenardi C, Haupt J, et al. (1998) Simulation of Berkovich nanoindentation experiments on thin films using finite element method. *Thin Solid Films* 312: 240–248. https://doi.org/10.1016/S0040-6090(97)00739-6
24. Wang K, Ma Q, Xu L, et al. (2023) Determining the elastic–plastic properties of materials with residual stress included using nanoindentation experiments and dimensionless functions. *Eng Fract Mech* 282: 109175. https://doi.org/10.1016/j.engfracmech.2023.109175
25. Noii N, Aghayan I (2019) Characterization of elastic-plastic coated material properties by indentation techniques using optimisation algorithms and finite element analysis. *Int J Mech Sci* 152: 465–480. https://doi.org/10.1016/j.ijmecsci.2019.01.010
26. Kang JJ, Becker AA, Sun W (2012) Determining elastic–plastic properties from indentation data obtained from finite element simulations and experimental results. *Int J Mech Sci* 62: 34–46. https://doi.org/10.1016/j.ijmecsci.2012.05.011
27. Kang JJ, Becker AA, Wen W, et al. (2018) Extracting elastic-plastic properties from experimental loading-unloading indentation curves using different optimization techniques. *Int J Mech Sci* 144: 102–109. https://doi.org/10.1016/j.ijmecsci.2018.05.043
28. Shaoming M, Sun Y, Wang H, et al. (2017) Effect of a minor Sr modifier on the microstructures and mechanical properties of 7075 T6 Al alloys. *Metals* 7: 13. https://doi.org/10.3390/met7010013

29. Zhou B, Lui B, Zhang S, et al. (2021) Microstructure evolution of recycled 7075 aluminum alloy and its mechanical and corrosion properties. *J Alloys Compd* 879: 160407. https://doi.org/10.1016/j.jallcom.2021.160407
30. Pastor A, Svoboda G (2013) Time-evolution of heat affected zone (HAZ) of friction stir welds of AA7075-T651. *J Mater Phys Chem* 1: 58–64. https://doi.org/10.12691/jmpc-1-4-1
31. Krzak-Ros J, Filipiak J, Pezowicz C, et al. (2009) The effect of substrate roughness on the surface structure of TiO_2, SiO_2, and doped thin films prepared by the sol-gel method. *Acta Bioeng Biomech* 11: 21–9.
32. Chuang LC, Luo CH (2011) Nanomechanical properties of prepared-TiO_2 films using nanoindentation technique. *Adv Mat Res* 214: 388–391. https://doi.org/10.4028/www.scientific.net/AMR.214.388
33. Bastakys L, Marcinauskas L, Milieska M, et al. (2023) Tribological properties of Cr_2O_3, Cr_2O_3–SiO_2-TiO_2 and Cr_2O_3–SiO_2-TiO_2-graphite coatings deposited by atmospheric plasma spraying. *Coatings* 13: 408. https://doi.org/10.3390/coatings13020408
34. Chuang LC, Luo CH, Yang SH (2011) The structure and mechanical properties of thick rutile-TiO_2 films using different coating treatments. *Appl Surf Sci* 258: 297–303. https://doi.org/10.1016/j.apsusc.2011.08.055
35. Boshkova N, Stambolova I, Stoyanova D, et al. (2023) Protective characteristics of TiO_2 sol-gel layer deposited on Zn-Ni or Zn-Co substrates. *Coatings* 13: 295. https://doi.org/10.3390/coatings13020295
36. Rivero PJ, Maeztu JD, Berlanga C, et al. (2018) Hydrophobic and corrosion behavior of sol-gel hybrid coatings based on the combination of TiO NPs and fluorinated chains for aluminum alloys protection. *Metals* 8: 1076. https://doi.org/10.3390/met8121076
37. Shadravan A, Sadeghian Z, Nemati A, et al. (2015) Corrosion protection of 1050 aluminum alloy using a smart self-cleaning TiO_2-CNT coating. *Surf Coat Technol* 275: 224–231. https://doi.org/10.1016/j.surfcoat.2015.05.015

AIMS Press